Chapter 2
Interactions with the Atmosphere and Road

2.1 Introduction

The interactions of a car with its environment—gravity, the atmosphere, and the road surface—create forces which act on the car, usually opposing its motion. This chapter shows how these forces are related to the characteristics of the car under the designer's control, such as its shape and weight, and to the effort required to move it: the tractive force. A magnitude will be calculated to give the reader an idea of the importance of each interaction. The calculations will use the characteristics of actual solar racing cars to make the numbers realistic.

No attempt is made to present an exhaustive treatment of each interaction. However, the most important features have been presented. Additional details will be found in Chaps. 17, 18, 19 and 20. Readers who wish to pursue topics in even greater depth may consult the references at the end of the chapter.

Cruise Condition This chapter concentrates on the interactions going on most of the time, which will be called the *cruise condition*. The cruise condition plays the strongest role in setting the energy consumption of the car, which determines the range. In this condition, the car moves straight ahead or turns through a large-enough radius or at a slow-enough angular rate, such that inertia-related forces transverse to the car's direction of motion are relatively small. Also, the wind relative to the car, which interacts with the shape of the car to create aerodynamic forces, blows from nearly directly ahead. The aerodynamic side forces are therefore relatively small. Thus, in the cruise condition all inertial and aerodynamic forces acting transverse to the direction of motion, and their associated moments, are neglected.

Intermittent Conditions However, important interactions are associated with events that happen intermittently, such as side gusts and emergency maneuvers. The transverse forces generated in these events strongly influence the controllability, stability, and structural design of a solar-electric vehicle.

When passed by a large vehicle, such as a truck, or when a wind gust blows suddenly from the side, a car experiences wind forces which tend to blow it sideways and rotate it about the vertical axis through its center of gravity. Solar racing cars

E. F. Thacher, *A Solar Car Primer,* DOI 10.1007/978-3-319-17494-5_2

tend to be light and are thus more sensitive to side gusts than conventional vehicles. Chapter 21, *Stability Calculations,* presents a method for predicting the effect of a side gust.

A solar car maneuvering in an emergency may be required to accelerate or brake while turning. In this situation, the car should remain controllable[1] and hence must not skid nor roll over, and its structure must withstand the moments and forces developed by the maneuver. Chapter 21 presents an analysis of the stability of the vehicle.

2.2 Equivalent Interactions

The forces on the car are distributed over the car or some portion of it. Gravity acts on the entire mass of the car. The friction force of the road on the tires acts over the area of the tire in contact with the road. In general, each force tends to both translate the car in and rotate the car about, at least one coordinate direction. To conveniently model the dynamics and energetics of the vehicle, we replace each distributed force by an equivalent isolated force and its associated moment. That is, the isolated force and moment have the same translational and rotational effects as the distributed force which they replace. Each of the equivalent forces acts at a convenient point, such as the center of gravity. Each of the equivalent moments acts about a convenient axis (usually a coordinate axis). Henceforward when the terms "force" and "moment" are used, it will usually be the equivalent, isolated forces and moments that are meant.

2.3 Coordinate Systems

Figure 2.1 shows a set of coordinate axes attached to the center of gravity of a solar-electric car so that the axes always point in the same directions relative to the car. The positive direction of each axis is shown. A force acting in the positive direction of each axis is defined as positive. A semicircular arrow about each coordinate axis shows the positive direction of the moments about those axes.

Aerodynamic forces arise from the motion of the air relative to the car. Thus, it is natural when discussing this relative motion to think of the car as stationary with axes attached to it. This is exactly the situation when the aerodynamic forces are measured in a wind tunnel, for instance. When it is more convenient, we will revert to thinking of the car as moving with respect to a coordinate system fixed to the earth, such as at the starting line at the Indianapolis Motor Speedway.

[1] Within specified design limits; absolute stability cannot be achieved.

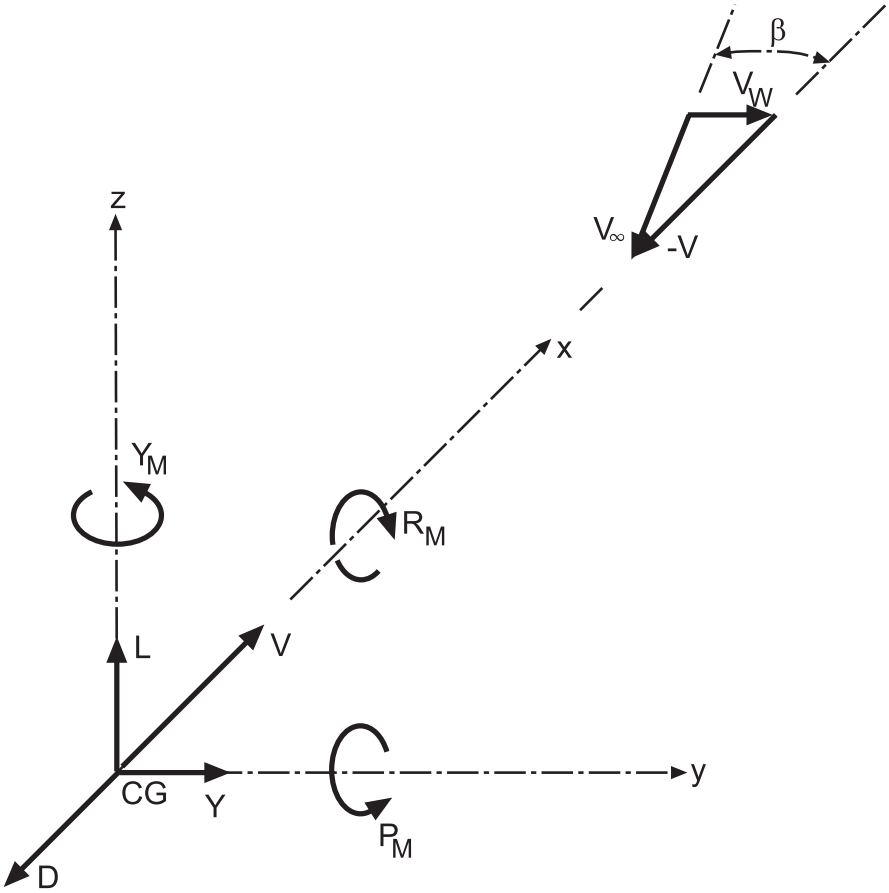

Fig. 2.1 Coordinate axes

2.4 Aerodynamic Interactions

We will select the point of action of aerodynamic forces as the center of gravity of the vehicle. Wind tunnel measurements of the moments of these forces are by convention often referenced to a point on the centerline of the car and halfway down the wheelbase. However, it is convenient when discussing their effects on motion to reference these moments to the center of gravity, as for the forces.

Figure 2.1 shows three aerodynamic forces and three aerodynamic moments, a force and moment for each coordinate axis, each named to suggest how it tends to affect the car's motion. The force acting along the *x*-axis is called *drag (D),* that acting along the *y*-axis is called *side force (Y),* and that acting along the *z*-axis is called *lift (L)*. The moment about the *x*-axis is called *roll* (R_M), that about the *y*-axis is called *pitch* (P_M), and that about the *z*-axis is called *yaw* (Y_M). In general, each of the forces and moments can be positive or negative.

Figure 2.1 also shows a vector representing the result of subtracting the car's velocity *(V)* from the true wind vector. This result is the *relative wind*, V_R, the motion of the air relative to the car, but sufficiently far upstream of the car so that it is undisturbed by the shape of the car. The relative wind blows from a *yaw angle*, *β,* measured from the *x*-axis and positive in the direction of positive Y_M.

In the cruise condition, the side force, yawing moment, rolling moment, and yaw angle are zero. Pitch, drag, and lift remain. How these arise from interactions between the flow field relative to the car and the car's shape, attitude, and internal flow passages will now be discussed.

Drag Experiment This section elaborates a bit on an example in Sherman (1990). Suppose you stir a mixture of small pepper grains and water in a white cup (so you can see the grains and thus visualize the flow) and then remove the spoon. The whirling motion of the mixture persists but eventually slows to a stop. The persistence depends upon the fluid's *momentum,* which in turn depends on both the mass of the fluid and its rotational speed. One would expect the liquid metal mercury in an identical cup to whirl for a longer time than water.

The mixture does not whirl forever but comes to rest because the friction force caused by the *viscosity* of the fluid opposes the rotation. Viscosity measures a fluid's resistance to flowing relative to itself, just like your hands resist being rubbed against each other. As in that case, the friction force is tangent to the flow. All fluids have viscosity; in some, such as air, it is small and in others, such as honey, it is large. (Try the experiment with a cup of honey. The pepper will stay on the honey's surface, but it will still help to visualize the flow. The friction force could rotate a light cup in this case. Would this show that the force is tangential to the cup's inner surface?)

If you observe the pepper, you will see (especially if you have been able to impart mostly circular motion to the mixture) that the grains near the inner surface of the cup slow down first. It turns out that the mixture actually contacting the cup's surface is at a speed of zero, which is called the *no slip* condition. So the rotational speed of the mixture is zero at the cup surface but increases toward the center. (You may observe other motions as well.) Because the friction force is created when the fluid resists flowing relative to itself, the speed difference (or *gradient*) must be present to give the friction force.

The foregoing discussion will be of use in understanding the friction drag on a car moving through air.

Parked Car A car parked along a road in still air, like the pepper grains in the cup or a fish motionless in a pond, is immersed in a fluid: the atmosphere. This mixture of gases (about 75 % nitrogen and 25 % oxygen) presses on every part of the outside (and inside) of the car. This pressure force distribution is called *static* because the atmosphere is not moving relative to the car at any point on it.

The static pressure is not uniformly distributed over the body of the fish, being greater underneath it because of the greater depth. This is also true for the parked car. However, the density of water is about 850 times greater than that of air at standard conditions (temperature 298.15 K, pressure 101.325 kPa). Consequently, the maximum pressure difference across the car is on the order of 0.0002 atm. So, differences in height between parts of the car may be neglected and the static

pressure distribution taken as uniform over the car. Thus, the net static pressure force on the car is zero.

Moving Car As the car moves down the road, air flows over the surface of the car. This relative motion[2] changes the pressure distribution such that a net pressure force is created that opposes the car's motion. The external flow also applies a retarding tangential friction force to the car's surface, as in the stirred-cup experiment. Also, air flows through the car for ventilation. The net pressure loss in internal passages, caused by friction and the losses in ducting bends, dampers, and other components, also exerts a retarding force. It can be as much as 8–10% of the total.

The total of the external and internal retarding forces we call *drag*. The magnitude of the drag is expressed by

$$D = c_{\mathrm{D}} A_D q. \tag{2.1}$$

The drag coefficient, c_{D}, a dimensionless quantity, characterizes the drag of the car and changes with the flow, in general. The *dynamic pressure* of the relative air speed far from the car, q, is given by

$$q = \frac{1}{2}\rho V_{\mathrm{R}}^2. \tag{2.2}$$

The dynamic pressure is the pressure increase above the ambient static pressure that would occur if the flow were brought to a halt with no losses (stagnate) against a surface. The air density (ρ) may be computed from the ideal gas equation

$$\rho = \frac{p}{R_{\mathrm{A}} T}. \tag{2.3}$$

The gas constant for air (R_{A}) is 0.287 kJ/kg·K. At standard temperature and pressure, Eq. (2.3) gives an air density of 1.184 kg/m^3. Note that for the same pressure, the drag is lower if the air is hotter and higher if the air is cooler.

In order to give units of force, the dynamic pressure must be multiplied by an area. By convention, the area used is the profile area (A_D), the area blocked out by the car when viewed from straight ahead. The product $c_{\mathrm{D}}A_D$ is called the *drag area*. Chapter 17 presents a means of estimating the drag area of a candidate body shape. Measurement of the drag area of a scale model or full-scale vehicle in a wind tunnel or by coast-down testing will be discussed in Chap. 12, *Testing*.

The drag coefficient incorporates all of the opposing drag force components mentioned: friction (c_{F}), pressure (c_S), and ventilation (c_{V}). Referring each component to $A_D q$ gives

$$c_{\mathrm{D}} = c_{\mathrm{F}} + c_S + c_{\mathrm{V}}. \tag{2.4}$$

We shall now explain in more detail why these components arise.

[2] It is the relative motion that counts; you could also blow on a stationary car and create drag, as in a wind tunnel.

2.5 Friction Drag

Boundary Layer Suppose that the relative airflow approaching the car is smooth and at zero yaw angle ($\beta = 0$ in Fig. 2.1). Like the water–pepper mixture in the cup, the air at the car's surface moves at zero speed relative to that surface. However, air farther from the surface moves nearer to the relative speed of the surrounding air, as shown in Fig. 2.2 (in which the *n*-axis is the local vertical). The air layer over which the local relative flow speed changes from zero to 99 % of that of the surrounding air is defined as the *boundary layer*.

The boundary layer thickens as the distance from the front of the car increases. A velocity gradient now exists in a viscous fluid. Hence, the air applies a retarding frictional force tangent to the surface of the car. As the car increases speed, the gradient becomes steeper, and the friction force at the surface increases. Figure 2.2 shows the gradient at the surface as the slope ($\Delta V_R/\Delta n$) of the tangent to the velocity distribution at that point. The symbol τ_0 represents the friction force per unit surface area. The *streamlines* shown in Fig. 2.2 are imaginary lines tangent to the local flow velocity.

Viscosity As we expect from the cup experiment, the proportionality factor between friction force and the velocity gradient is the viscosity of the air *(μ)*.[3] If the car were moving through water, the viscosity of which is about 48 times that of air at 25 °C, the frictional drag would be much larger at a given speed (remember the honey). Near atmospheric pressure, the viscosity of air shows a weak tendency to

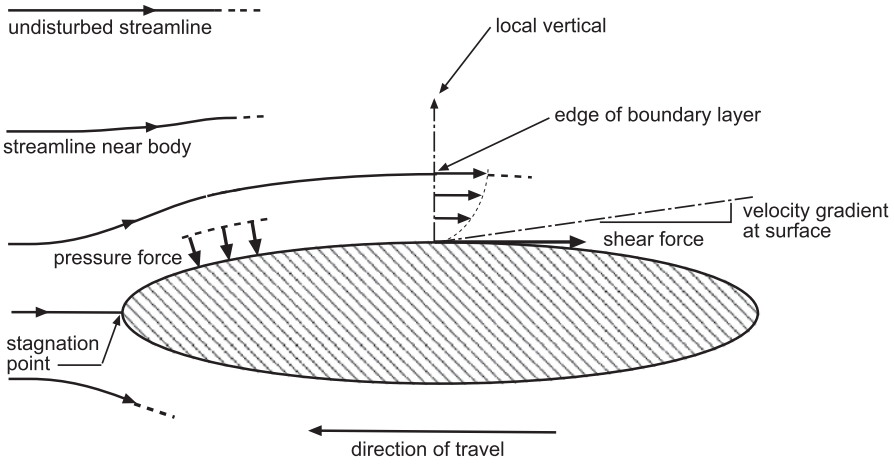

Fig. 2.2 Boundary layer and aerodynamic forces

[3] Many fluids obey this relation between the surface shear force and the velocity gradient, air and water, for instance. Such fluids are called newtonian, after Sir Isaac Newton, who first proposed this linear model.

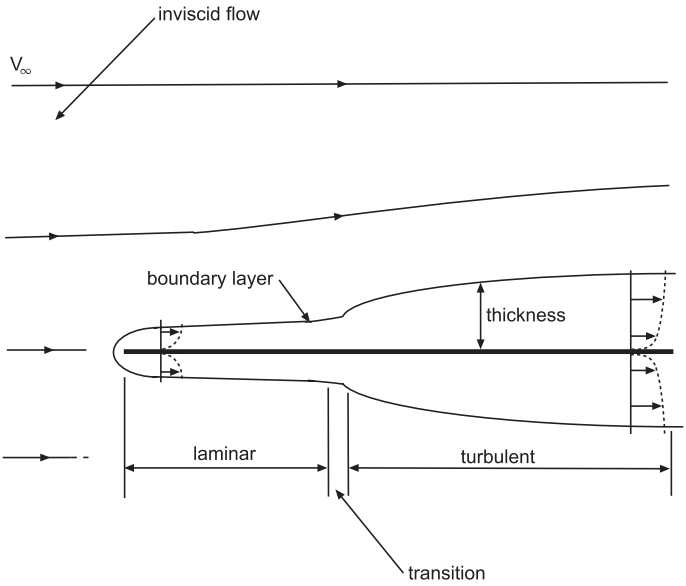

Fig. 2.3 Laminar and turbulent boundary layers

increase with pressure and a strong tendency to increase with temperature. Thus, the frictional drag increases with increasing temperature.

Is this the whole story of friction drag? No, unfortunately; we are headed for more trouble as we increase speed.

Laminar and Turbulent Flow Figure 2.3 shows a smooth, flat plate traversed by initially smooth air flow.

The flow contacts the plate, and the boundary layer forms. The flow in the boundary layer at this early stage is still smooth. We can visualize this as very thin air layers, *lamina,* moving relative to each other with no velocity components transverse to their motion. The flow is called *laminar* because of this characteristic. A particle of air striking, say, a small bump (no actual surface can be exactly smooth) may deflect up a bit, but the viscous friction of the other particles drags it back into line, keeping the flow laminar.

An impulsive force was applied between the fluid and the surface when the element glanced off the little bump and thereby gained momentum away from the surface. Further on, at the next bump (or other disturbance, maybe even loud rock music), the thickening of the boundary layer has magnified the destabilizing impulse force relative to the stabilizing viscous force because the velocity gradient is reduced. So, as the boundary layer thickens, small waves appear in it. The waves grow into chaotic eddies and the boundary layer makes a transition to *turbulence,* accompanied by additional thickening.

Besides the torque need to overcome the viscous friction, the engine of the car must now exert extra torque on the driving wheel or wheels to cause the eddies to circulate. Consequently, the friction drag in turbulent flow is higher than in laminar flow.

Reynolds Number The foregoing discussion implies that a number correlated with the ratio of the impulsive to viscous forces in the boundary layer would also correlate strongly with the transition to turbulence. Because force is proportional to the rate of change of the momentum, we expect the impulsive force will be correlated with the momentum flow rate of the air external to the boundary layer. This is ρV_R^2, when expressed as force per unit area perpendicular to the flow, or $\rho V_R^2 A_{flow}$ in force units, where A_{flow} is a conveniently chosen reference area perpendicular to the flow. The friction drag per unit surface area is proportional to $\mu V_R/\ell$, where ℓ is the local boundary layer thickness and A_{fric} is a reference area on the car's surface. Since $\ell A_{flow}/A_{fric}$ has units of length and A_{flow} and A_{fric} are arbitrary, the ratio of interest is:

$$\mathrm{Re}_\lambda = \frac{\rho V_R \lambda}{\mu}, \tag{2.5}$$

where λ stands for a conveniently chosen reference length. Equation (2.5) defines the *Reynolds number*. For the present discussion, we choose the distance x from the nose of the car to a point in the boundary layer measured along the surface as the characteristic length because the thickening of the boundary layer depends on the distance from the nose.[4] The number, now called the *local* Reynolds number because it depends upon the location, is:

$$\mathrm{Re}_x = \frac{\rho V_R x}{\mu}. \tag{2.6}$$

The local Reynolds number at which the transition to turbulence begins on the surface is called the *critical* local Reynolds number. This number is usually found by experiment. The transition to turbulence is affected by the roughness of the surface: the rougher the plate, the lower the critical Reynolds number at which it begins. On the other hand, as Eq. 2.6 implies, for a given fluid and surface, the critical Reynolds number will be reached at a shorter distance from the nose when the flow is faster.

Thickness Compared to the characteristic dimension of the body in the flow direction, say the length of the plate in Fig. 2.3, the boundary layer is quite thin, even in turbulent flow. Suppose the length of the plate were 2 m and the latter portion of its surface were in turbulent flow, as shown, the boundary layer thickness would be only of the order of 4 cm at the trailing edge. (Its dimensions have been exaggerated in the figures.) Nevertheless, all of the viscous interaction of the airflow with a body takes place in the boundary layer. Compared to the boundary layer, the flow external to this layer may be treated as if it had no viscosity.

Total Friction Drag Because the local frictional force discussed above is expressed as a force per unit area, the total frictional force on the car is proportional to the surface area of the car. The larger this area, the larger the force will be. However, the

[4] The Reynolds number is important in other contexts. So, other reference lengths more appropriate for the context are defined for these cases.

line of action of the drag force is antiparallel to the direction of motion. Therefore, the friction force at a particular location contributes to the drag in proportion as the surface upon which it acts is parallel to the direction of motion. The flow over the upstream face of a rear-view mirror is nearly perpendicular to the direction of motion and therefore contributes little to the total friction drag force, for example. It contributes to the pressure drag, however, as the following discussion demonstrates.

2.6 Pressure Drag

Frictionless Flow We now return to the effect of shape on pressure. Figure 2.4 shows a cross-sectional view of the steady flow of air over two smooth cylinders. Both are very long compared to their diameters, so the complicating effect of flow near their ends may be neglected. Consider first the flow over the upper cylinder, for which we imagine the viscosity of the air to be zero, so that the flow is frictionless.[5]

Since a streamline is an imaginary line tangent to the local flow velocity, if the flow is undisturbed, all the streamlines are parallel and flat. Note that, by definition, flow cannot cross a streamline. Now we can imagine that the upper half of the cylinder is in a channel.[6] The upper "wall" of this channel is a surface formed by the streamlines of air far enough from the cylinder to be undisturbed by its presence. These bounding streamlines, taken together, could be called a *stream surface*. The lower wall is formed by the stream surface that hits the front of the cylinder and then follows its surface.

Bernoulli's Equation Consider any streamline between two vertical planes, such as those marked 1 and 2 in the figure. The flow is steady, there is no friction and, we assume, no heating of the air. Then it is true that for any two points along the streamline

$$\frac{p_1}{\rho_1}+\frac{V_1^2}{2}+gZ_1-\left(\frac{p_2}{\rho_2}+\frac{V_2^2}{2}+gZ_2\right)=0. \tag{2.7}$$

Equation (2.7), called *Bernoulli's equation,* shows that

$$\frac{p}{\rho}+\frac{V^2}{2}+gZ=const. \tag{2.8}$$

along a streamline for the conditions assumed. Now, to unclutter things even more, we observe that the gravitational potential energy term, gZ, may be neglected for height changes on the order of the height of an automobile or truck. Also, if the flow were incompressible, the density, ρ, would be constant and then the quantity

[5] This apparently oversimplified scenario will still yield valid insights, believe it or not.

[6] Actually, we could equally well imagine the entire cylinder in a channel, but the drawing of a half cylinder takes up less space.

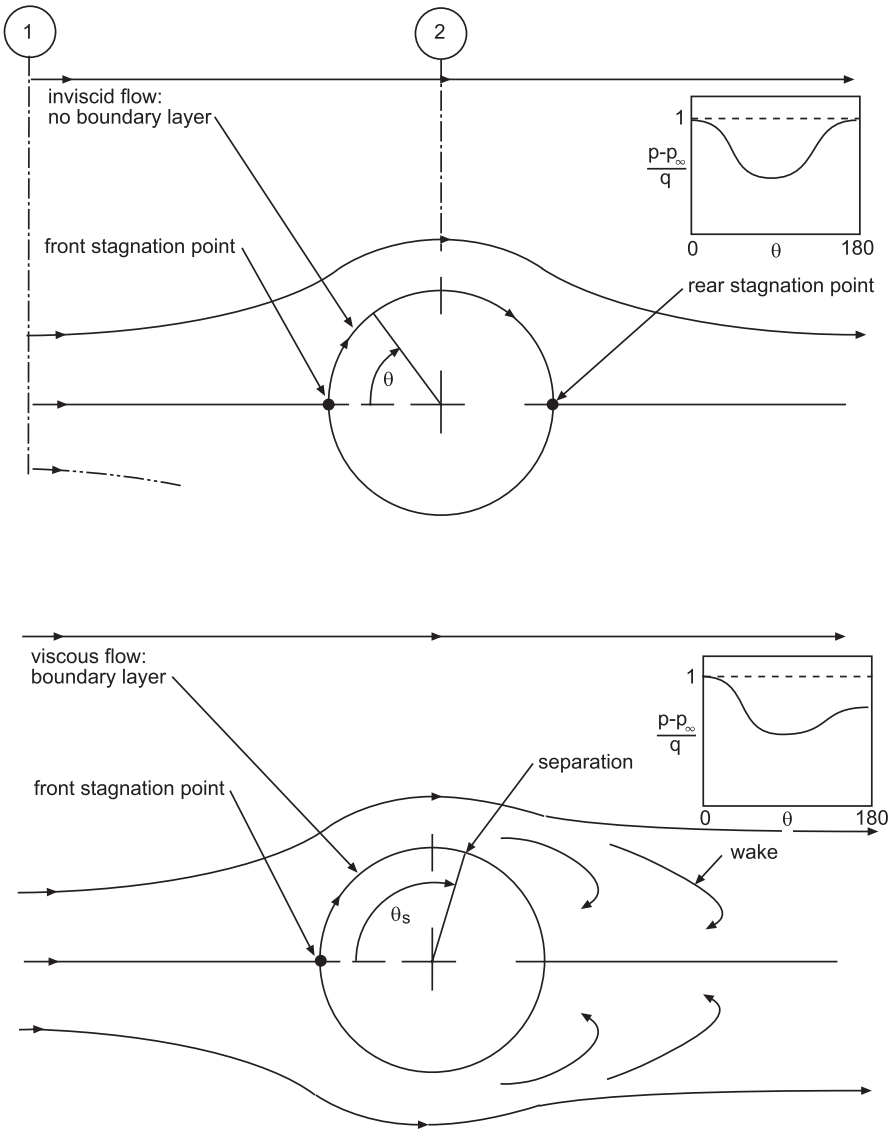

Fig. 2.4 Origin of pressure drag

$p+\rho V^2/2$, the *total pressure*, p_0, would be constant along a streamline. The pressure changes typical of external air flows produce only small changes in density. We will model such flows as incompressible.

Using our simple model, let us investigate the static pressure distribution on the upper cylinder of Fig. 2.4. Upstream of the disturbance of the cylinder, the velocity is uniform (all streamlines flat, parallel, and evenly spaced). Therefore, the pressure is uniform in the flow. At the forward-most point (θ=0° in the figure), the air

speed is momentarily zero, so it is a stagnation point (even though it is really a line) and $p=p_0$. The flow then turns and moves up, tangent to the cylinder's surface. Hence, because the mass flow rate is steady and the density cannot change, the air speed increases to a maximum, and, as required by Bernoulli's equation, the static pressure decreases to a minimum as the point of minimum channel cross-sectional area at the top of the cylinder ($\theta=90°$). Beyond this point, the air speed decreases and the static pressure increases. At the downstream location opposite to the front stagnation point ($\theta=180°$), the tangential air speed component becomes zero. A rear stagnation point forms at which $p=p_0$ once again.

Figure 2.4 shows the pressure variation around the cylinder. Clearly the shape of the cylinder strongly influences the pressure distribution over it. But notice, there is no net pressure change across it in the flow direction for the ideal, frictionless conditions assumed. Therefore, there is no pressure drag.

Flow with Friction Pressure drag on objects immersed in a real, viscous fluid arises because of *boundary layer separation*. Consider the lower cylinder of Fig. 2.4, which is immersed in a real, viscous, approximately incompressible fluid such as air. A boundary layer now forms on the cylinder. Bernoulli's equation is invalid inside the boundary layer. But because, as we observed earlier, the flow external to the boundary layer is approximately frictionless and the boundary layer is quite thin, the pressure imposed on the boundary layer approximately obeys Bernoulli's law. The pressure increase on the downstream surface of the lower cylinder of Fig. 2.4 opposes the flow in the layer. The more sharply the surface curves down, the more rapid will be the opposing pressure increase predicted by Bernoulli's equation. At some position angle, this causes the velocity gradient at the surface to be zero.[7] At that point, the main flow ceases to follow the curved surface, and the boundary layer is said to *separate* from that surface. The flow then forms a turbulent wake, as shown. This causes the air pressure on the rear surface downstream of the separation area to drop below that near the front stagnation point and perhaps even below that of the ambient air. There is now a pressure force difference, high in front, low in back. This net opposing force is called *pressure drag* (or sometimes *profile drag*). Pressure or profile drag is reduced by making the shape less blunt.

Streamlining Figure 2.5 shows a cylindrically shaped body and a streamlined airfoil-shaped body, both with circular cross sections and having the same profile area. The drawing of the cylindrically shaped body shows that separation can occur at locations upstream of the trailing surface, such as at the forward corners of the box shape. Downstream of these locations, the flow may reattach to the car and some pressure loss be recovered.[8] Compare the cylindrical shape to the streamlined shape which minimizes separation and thus pressure drag, by avoiding rapid changes in the slope of its surface.

Qualitative pressure and friction force profiles for the two shapes are shown at the bottom of the figure (tear drop: dashed line). These curves were constructed using the exchange of pressure and velocity expressed in the Bernoulli equation.

[7] There will even be back flow downstream of the separation point.

[8] These local zones of separated flow are called separation bubbles.

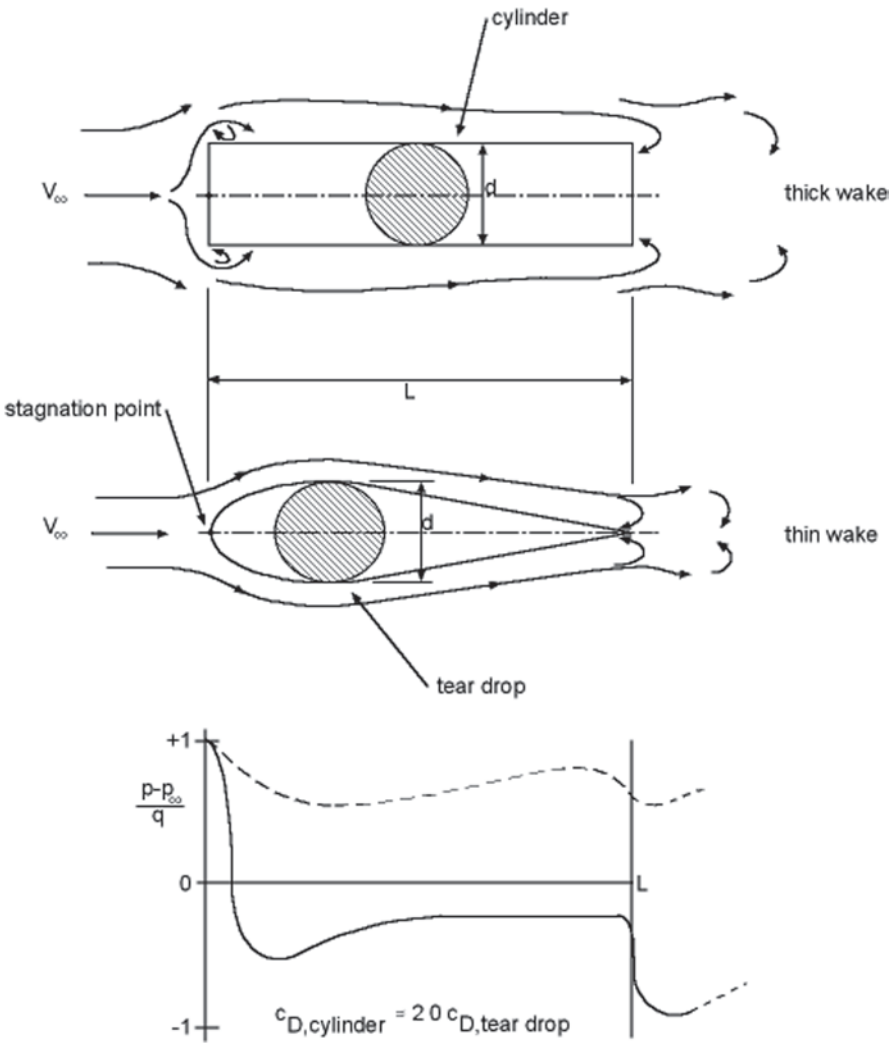

Fig. 2.5 Effect of streamlining

The velocity gradient at the surface in separated zones is small and therefore so is the shear force. However, streamlining may add to the external area that contributes to friction drag because, by filling in the areas having more abrupt slope changes, streamlining increases the component of surface area parallel to the direction of motion. Thus, there would seem to be a trade-off between pressure and friction drag. But separation usually dominates the drag from external flow (Hucho 1983). Hence, any gains in friction drag from streamlining are usually outweighed by the reduction in pressure drag. Nevertheless, one should bear in mind that solar racing cars are radically streamlined to give very low total drag. Friction drag is therefore of greater relative importance than in conventional vehicles. Pay close attention to details such as surface finish; in solar racing cars, the drag is in the details.

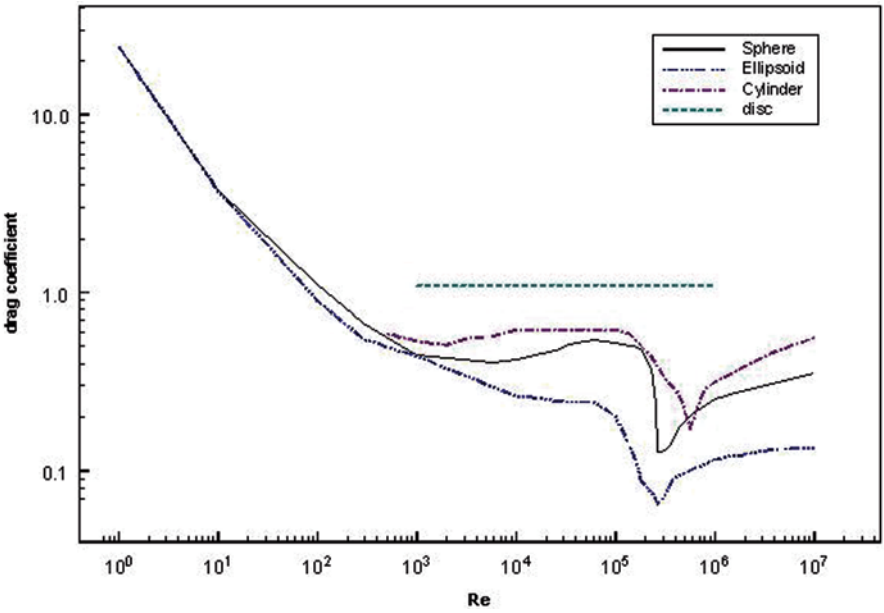

Fig. 2.6 Drag coefficients of four shapes. (Adapted from White 1986)

Total Pressure Drag The total pressure drag may be found in principle by adding the components of the local normal pressure force (pressure times area) in the direction of motion. Applying this rule to the shapes of Fig. 2.5, we see that the retarding and pushing components of the pressure force tend to be concentrated at the front and rear of the car (except for the "separation bubbles" mentioned in footnote 8).

Effect of Turbulence Turbulence in the boundary layer can reduce the total drag on a body, even though it increases the friction drag in non-separated portions of the boundary layer. Figure 2.6 illustrates this effect for the total drag of a disk, cylinder, ellipsoid, and sphere in cross flow. The curves are similar, except for that of the disc. In laminar creeping flow only friction is present, then laminar separation occurs, and the drag coefficient becomes nearly constant. Observe that the disk's drag is almost completely determined by separation because it has little surface area parallel to the flow, so that at most Reynolds numbers viscous boundary layer effects are negligible. However, boundary layers can develop on the other three objects. Turbulence begins on these shapes at about a Reynolds number of 10^5, where the drag coefficient drops. The increased momentum in the boundary layer causes the ring-shaped locus of separated flow to be blown farther downstream. Thus, the region of low pressure on the downstream side of the cylinder is smaller and the drag force is lower. After the transition to turbulence is complete, the drag coefficient slowly increases with the Reynolds number because of friction.

The drag-reducing effect of turbulence is employed in the manufacture of golf balls. The dimples on the surface of a golf ball tend to "trip" the flow to turbulence, thus reducing drag and increasing the distance the ball carries. This technique of introducing local roughness to trip the flow has been employed on solar racing cars to reduce the drag of the cockpit canopy.

Local wakes may be formed when the shape of the car forces flows of differing speeds to join, imparting a whirling *(vortex)* motion to the resulting flow. The low pressure in the vortex results in an additional drag. The section on lift explains how merging flows of differing speeds can be created.

2.7 Estimating Drag

The drag area (and drag coefficient) of a proposed vehicle may be estimated by summing the drag areas of the components that make up the vehicle's shape. The free air drag coefficients of the shape components must be known and corrections for ground effect and interference must be applied. This *drag build-up* method is capable of estimates that agree within ± 10 % with the drag areas measured in wind tunnel tests. Chapter 17 explains this method and Chap. 9, *Solar Racer: Concept Generation and Selection,* presents a detailed application of it.

2.8 Ventilation Drag

Ventilation of the cockpit forces out the hot, stale air, helping to keep the cockpit comfortable. Outside air supplied to the battery compartment flushes out gases evolved by the battery during charging. These might accumulate in the battery compartment in explosive amounts if it were sealed. Race regulations (Chap. 16) require a certain fan-forced airflow through the battery compartment whenever the battery is electrically connected to the solar car.

Sample System Figure 2.7 shows a ventilation system layout schematically. The air enters in the front of the car through a low-loss (round-edged) inlet. It flows through the cockpit (simplified to a box-shaped volume), the battery box, the fan, a diffuser, and then leaves the car. The diffuser increases the pressure of the flow before returning it to the outside. Heat inputs from the sun, instruments, and the driver, and heat losses to the outside are shown. These cannot be neglected as they were in deriving Eq. (2.7).

Drag Sources The internal flow drag arises in a manner similar to that from external flow. Consider Fig. 2.7. The internal flow applies viscous shear forces to the inside surfaces of the air ducts. The rougher the surface, the greater the force. The pressure increases as the flow velocity decreases in the sudden expansion when the air is discharged into the cockpit. Separation occurs, as shown, dissipating some energy and thereby reducing the pressure increase. This causes drag, in effect, by increasing the net pressure drop in the system. Separation in the sudden contraction at the discharge from the cockpit increases the pressure drop caused by the area decrease. Separation also can occur in the diffuser if its included angle is too large, reducing the pressure recovery as in the sudden expansion. The pressure loss in the

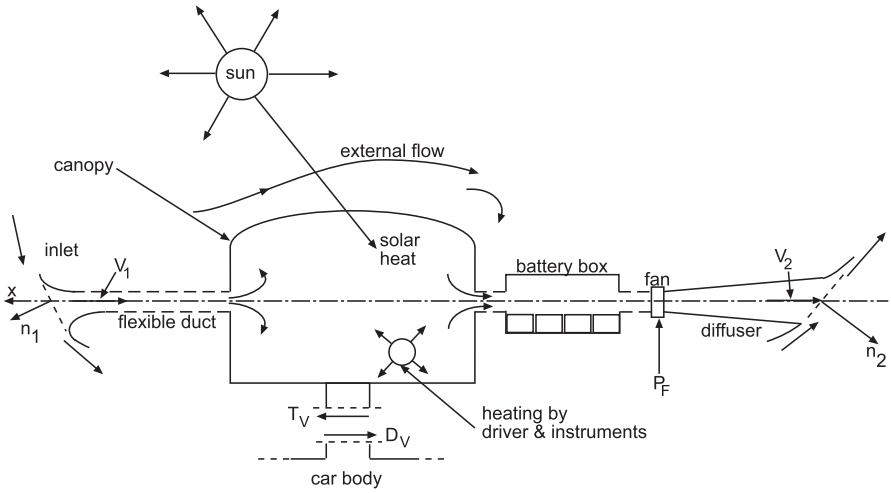

Fig. 2.7 A ventilation system

duct is reduced by the pressure increase across the fan. Note that race rules require the fan to be running when the battery is connected to the main bus.

Drag Force The locations where the system is attached to the car are symbolized by the single pylon. It has been cut to show the x-direction tractive force (T_V) exerted at the support. To find the drag, D_V, at a steady speed, sum the forces in the x-direction on the free body consisting of the ventilation system and the air in it and, following Newton's second law, equate this sum to the momentum change of the air between the inlet and outlet. Then note that $D_V = -T_V$. The drag on the ventilation system is transmitted through the pylon to the body of the car. Consequently, the motor must supply additional tractive force equal to D_V. If m_1 represents the mass flow rate through the ventilation system, the drag then is:

$$D_V = (\overline{p}_{G1} A_1 - \overline{p}_{G2} A_2)_X + \dot{m}_1 (V_1 - V_2)_X . \tag{2.9}$$

In general, the pressure over the inlet and outlet openings will not be uniform. Hence, the average gauge pressures over the inlet and outlet, $\overline{p}_{G1}$ and $\overline{p}_{G2}$, respectively, must be estimated from information about the flow around the car. The "x" subscript denotes components in the x-direction.

The ventilation drag coefficient is computed from the drag force as:

$$c_V = \frac{D_V}{qA_D} . \tag{2.10}$$

A method for estimating the ventilation flow rate and for sizing the fans used in the system is explained in Chap. 18. An application of this method and of Eqs. 2.9 and 2.10, to estimate the drag caused by the ventilation flow, is presented in Chap. 10, *Solar Racer: Detailed Design*.

2.9 Lift

Lift is directed perpendicular to the *x, y* plane, the plane of the car's motion. As mentioned above, the net lift force is not necessarily upward. The lift coefficient, defined as

$$c_{\mathrm{L}} = \frac{L}{qA_D}, \tag{2.11}$$

may therefore be positive or negative.

Ground Effect Figure 2.8 shows three views of a simplified solar car body. It has a symmetric airfoil shape longitudinally, is elliptic in cross section, and in plan view rounded in front and square in back. The angle between the horizontal and the chord line connecting the nose and the tail of the car we shall call the *pitch angle,* positive when up. Figure 2.8 shows the car at zero pitch. Underneath the drawing is a graph showing qualitatively the pressure distribution around the car.

The plot below the drawing shows that even though the pitch is zero and the shape is symmetric about the chord line, the pressure distribution on the underside of the car (dashed line) differs from that on the top (solid line). This is because of the proximity of the road surface. The variable cross-sectional area channel formed by the road and the car's underbody alters the speed and pressure distribution as required by the Bernoulli equation. The arrows indicate the direction and magnitude of the lift, with the large arrows showing that the lift causes a net upward pitching moment about the center of gravity (L_{CG}).

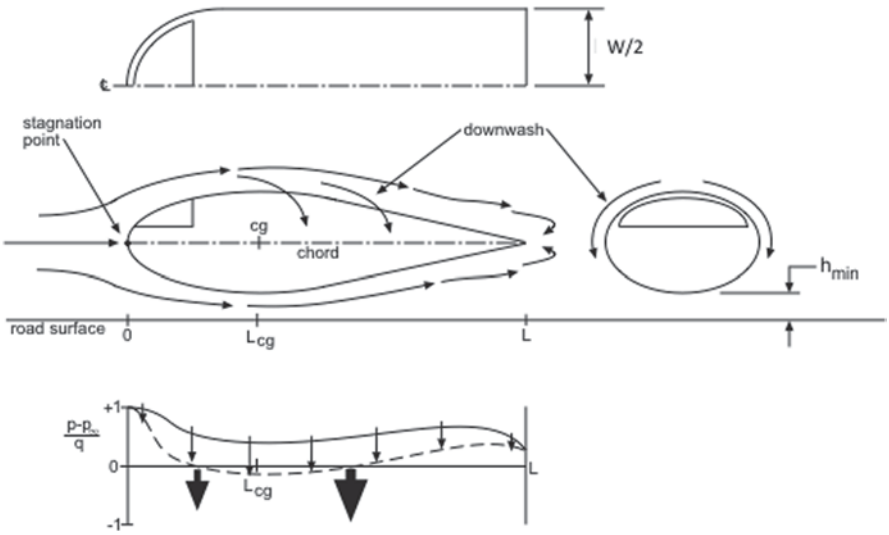

Fig. 2.8 Ground effect

If the pitch angle were made positive, the lift might become net positive because the stagnation point would shift underneath the car. If the pitch angle were made negative, the stagnation point could shift to the top of the car. A net negative pitching moment may occur.

Note in Fig. 2.8 that because of the pressure difference between the top and bottom of the car, flow from one side of the car can curl around and join the flow on the other side. This is called *upwash* or *downwash,* as appropriate. If the joining flows have different speeds, vortices may form and trail downwind. As explained in the pressure drag section, this is a source of drag. Upwash or downwash is associated with the lift distribution even when the net lift is nearly zero. However, the drag induced by each lift-induced vortex always adds to the total. Some lift is inescapable. The key to reducing vortex-induced drag is to smooth the joining of the flows. For example, use fillets at the junction of the body and fairings used to streamline exposed wheels. Chapter 17 gives rules for selecting the fillet radius and length.

Optimum Ground Clearance Morelli (1983) conducted wind tunnel tests on model shapes configured for low drag near the ground. His results showed that as the ratio h_{MIN}/W between the minimum height above the ground and the width of the car increased from the minimum value tested, near 0.05, to values of 1.0 or greater, the drag decreased, in some cases passed through a minimum that was less than the free-air value, and then approached free-air values as the influence of the tunnel floor on the pressure distribution diminished. These results may be contrasted with those Morelli presented for teardrop shapes which exhibited drag coefficients several times those of the special shapes at the same ground clearance ratios.

Study the "Shark" curves in Fig. 17.8. The lowest drag coefficient Morelli reported was about 0.045 for a 6.9% camber ratio (b_{max}/W) at a dimensionless ground clearance (h_{min}/W) of about 0.15. (This is the lowest of the three Shark's shapes tested.) For a 2-m wide car, this implies an actual minimum ground clearance of about 0.3 m. The teardrop shape's drag is not comparable to the Sharks until a clearance ratio of about 0.7. This corresponds to a clearance of 1.4 m for a 2-m wide car. Thus, the Morelli shape can have low drag without having to reduce roll stability by raising the clearance ratio. This is not true for the teardrop.

2.10 Example 2.1

Suppose a solar car (pitch angle −0.5°, profile area 1.46 m^2) is traveling at 96 kph (60 mph) in the cruise condition in still air at standard temperature and pressure. Under these conditions, c_D, and c_L are, respectively, 0.095 and 0.22. What are the drag and lift forces?

Solution The air density is:

$$\rho = \frac{101.325\frac{\text{kN}}{\text{m}^2}}{\left(0.287\frac{\text{kN}\cdot m}{\text{kg}\cdot K}\right)(298.15K)} = 1.184\frac{\text{kg}}{\text{m}^3}.$$

Dynamic pressure-profile area product (speed in m/s) then is:

$$q = \frac{1}{2}\left(1.184\frac{\text{kg}}{\text{m}^3}\right)\left(26.39\frac{\text{m}}{\text{s}}\right)^2 (1.46\text{m}^2) = 607.6\text{N}.$$

And the drag force becomes

$$D = (0.095)(607.6\text{N}) = 57.7\text{N},$$

directed opposite to the direction of motion. The lift is:

$$L = (0.22)(607.6\text{N}) = 133.7\text{N},$$

directed vertically up.

2.11 Pitch

The pitching moment, P_{M}, arises from the tendency of the lift distribution to rotate the car about the *y*-axis. The net lifting force may be nearly zero. But there still may be a lift-caused pitching moment.

The pitching moment coefficient is defined similarly to those of lift and drag, except that a length scale must be introduced into the denominator to non-dimensionalize the quotient. It is:

$$c_{P_{\text{M}}} = \frac{P_{\text{M}}}{qA_D L_{\text{W}}}. \tag{2.12}$$

2.12 Example 2.2

A wheel base length of 3.073 m will be used as the length scale in this example. For the conditions of Example 2.1, the pitching moment coefficient, $c_{P_{\text{M}}}$, is −0.196 about the *y*-axis through the center of gravity. Find the pitching moment.

Solution Using Eq. (2.13) gives

$$P_{\text{M}} = (-0.196)(607.6\text{N})(3.073\text{m}) = -366\text{N}\cdot\text{m}.$$

The negative sign denotes pitch down.

Pitch angle changes of a fraction of a degree regularly occur in the cruise condition. But in an emergency situation, such as a rear tire blow out in a three-wheeled car while cornering, a pitch up condition of two or three degrees might occur. At

highway speeds, this can cause a positive pitching moment in lightweight, airfoil-shaped vehicles sufficient to momentarily sharply reduce the normal force on one or both front wheel contact patches. During that moment, the driver has little or no steering control.[9]

2.13 Road and Gravity Interactions

Figure 2.9 shows a three-wheeled car moving up a straight grade in the cruise condition. The forces acting parallel or antiparallel to its motion are drag *(D),* rolling resistances (R_1, R_2, and R_3; numbered clockwise viewed from above starting with the left front wheel), the *x*-component of the weight *(W_X),* and the tractive force *(T)*. The tractive force is the force propelling the car up the hill. If the speed is steady, it equals the sum of the forces resisting motion. The forces acting normal to the direction of motion are lift *(L),* the *z*-component of the weight *(W_Z),* and the wheel reactions (N_1, N_2 and N_3). The pitching moment (P_M), shown positive, acts about the *y*-axis.

2.14 Gravity

The components of the weight of the car of Fig. 2.9 are

$$\begin{cases} W_x = W \sin\alpha \\ W_z = W \cos\alpha \end{cases}, \tag{2.13}$$

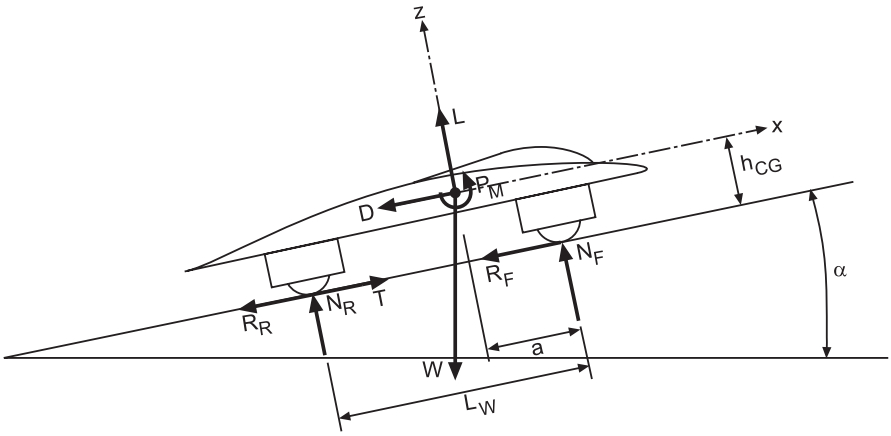

Fig. 2.9 Cruise condition forces and moments

[9] Clarkson University's 1995 Sunrayce car experienced this type of emergency at about 45 mph while running qualifying laps at the Indianapolis Raceway Park.

where W is the weight. Weight is the largest force on the car, in the cruise condition. W_x is the component of weight that directly opposes the motion when going up a hill (α positive) or aids the motion when descending a hill (α negative). The rolling resistance force is directly proportional to the vertical component of the weight W_Z, plus any up or down lift, as explained in the next section.

2.15 Example 2.3

Suppose the car of Fig. 2.9 weighs 3558.4 N and that the grade is 10%[10] (α of 5.71°). Find W_x and W_z.

Solution The component of weight opposing the motion up the hill would be:

$$W_x = (3558.4\text{N})\sin 5.71^\circ = 354.0\text{N}.$$

This force is a bit more than six times the drag force calculated in Example 2.1 for horizontal travel at 96 kph. The drag coefficient used in that example is typical of high-performance solar cars as reported by Storey et al. (1994). However, doubling of the drag coefficient, or halving of the grade, would still give an opposing weight component much larger than the drag in the example. The normal weight component is:

$$W_z = (3558.4\text{N})\cos 5.71^\circ = 3540.7\text{N}.$$

Range and Stability Reducing the weight improves the range of the vehicle by reducing the energy needed to overcome rolling resistance, accelerate, and climb hills. On the other hand, the stability of the car is also reduced because a lighter car is more sensitive to side wind gusts and side forces caused by turning.

2.16 Rolling Resistance

Dynamic Resistance Figure 2.10 shows a wheel in contact with the ground and moving straight ahead at speed V, like those of the car in Fig. 2.9. The tire deforms under load so that it contacts the road over an elliptically shaped[11] area called the *contact patch*. The tire is not sliding over the road, so there is no relative motion between the contact patch and the road's surface.

[10] In the first US cross-country solar car race, the solar cars were required to show that they could climb a 10% (rise/run times 100) grade.

[11] This deformed shape is typical of the small, high pressure, rounded-cross section tires usually used by solar racers.

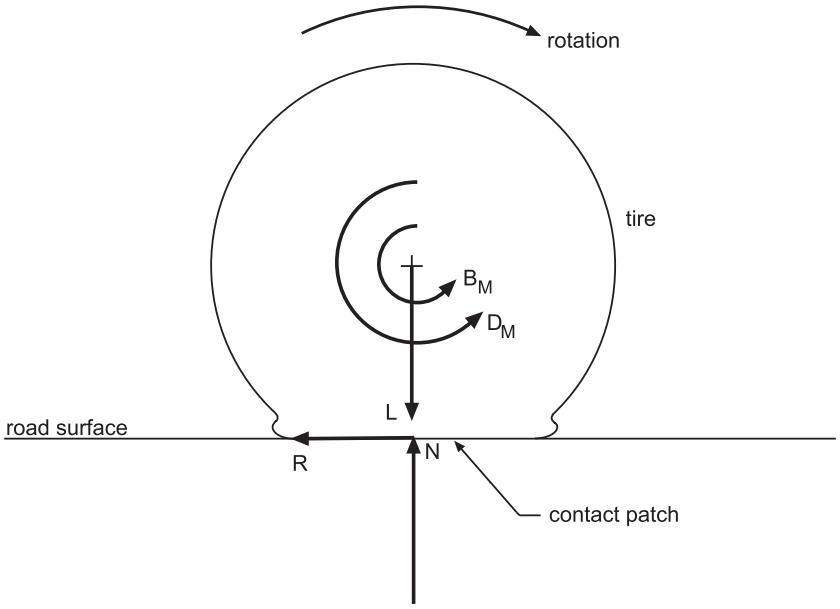

Fig. 2.10 Forces and moments on a wheel

We assume that the drag on the wheel caused by the flow over the car is accounted for in vehicle drag and focus on the drag resisting the wheel's rotation around its axis. A moment, D_M, about the wheel's axis opposing the wheel's rotation is imposed by the drag force created by the rotation of the wheel. The drag force is distributed over the wheel and depends upon the presence or absence of a wheel housing, the spacing between the wheel and its housing, and the flow field about the car. Another opposing moment, B_M, comes from friction in the wheel bearings. The moments may be represented by a moment-equivalent force applied to the contact patch acting on a moment arm attached to the axis of the wheel. We will call this force the *dynamic rolling resistance*.

Static Resistance As the tire rolls, the flexing of the tire needed to form the patch absorbs energy. The portion of the tire "flowing" into the leading edge of the patch is compressed, increasing the pressure on the leading edge above that caused by the weight. The portion of the tire leaving the contact patch expands, and most of the energy stored in the tire by the compression is recovered. However, the deformation is inelastic, so a portion of this energy is lost, manifesting itself as heating of the tire. Consequently, the contact pressure of the material leaving the contact patch is less than that entering the contact patch. The x-direction component of the net compressing force, F_C, on the material in the patch is called the *static rolling resistance.*

Total Resistance The *total rolling resistance*, *R,* is the sum of the static and moment-equivalent forces. The rolling resistance coefficient is defined as

Table 2.1 Rolling resistance coefficients

μ_1	μ_2 (h/km)	Source	Remark
0.00252	$3.14(10^{-5})$	Kyle 1990	Moulton 17 × 1 1/4 bicycle tire at 100 psig, $N = 100$ lbf; rotating drum test
0.0075–0.3	$3.11(10^{-5})$–0.0011	Steeds 1960	Typical μ_1 for automobile tires: lower value smooth pavement, higher unpaved

$$\mu = \frac{R}{N}. \tag{2.14}$$

We expect a dependence of μ on V through the dynamic component of resistance. Kyle (1990) and Steeds (1960) present models in which this coefficient is a linear function of V. SAE (1997) presents it as a function of V^2. The former model is adopted herein because it agrees with the test data of Kyle on small wheels typical of those used on solar racing cars. Also, it allows the dynamic coefficient to be easily separated from the drag area in coast-down testing, since otherwise both the dynamic rolling resistance and the drag would be functions of V^2.

The rolling resistance coefficient model adopted herein is:

$$\mu = \mu_1 + \mu_2 V. \tag{2.15}$$

When modeling the motion of the vehicle up a grade, the total load on the wheels is reduced to W_z, neglecting lift. Rolling resistance coefficients of tires are shown in Table 2.1.

2.17 Example 2.4

Suppose the vehicle of Fig. 2.9 were traveling 40 kph up the 10 % grade of Example 2.3. If it is equipped with the Moulton bicycle tires used in the drum test reported by Kyle, what would the total rolling resistance be?

Solution Using W_Z from Example 2.3 and Eqs. (2.14) and (2.15),

$$\mu = 0.00252 + (0.0000314\text{kph}^{-1})(40\text{kph}) = 0.00378,$$

$$R = (0.00378)(3540.7\text{N}) = 13.4\text{N},$$

where the lift has been neglected because of the low speed. The contact patch force accounts for 66 % of R.

Chapter 12, *Testing,* describes a method of measuring rolling resistance. Chapter 20 presents a method for estimating rolling resistance from tire properties during the design.

2.18 Tractive Force

The tractive force is the propulsive force equivalent to the torque delivered by the drive (the motor, controller, and transmission) to the driven wheels, or wheel. (Solar racing cars often have only one driven wheel. This reduces the weight, complexity, frictional losses, and cost of the car.) Suppose the radius of a driven wheel is r_W, and the flattening of the loaded tire is ignored. The equivalent tractive force is:

$$T = \frac{\tau}{r_W}. \tag{2.16}$$

2.19 Force Balance

At steady conditions (speed, weather, and road conditions independent of time), there is no acceleration, and so the sum of the forces in each coordinate direction must equal zero. And recall that in the cruise condition there is no force in the *y*-direction and consequently also no yawing moment. The force balance in the *x*-direction is:

$$T = D + W_x + R. \tag{2.17}$$

R is the total rolling resistance, related to the total normal force by Eq. (2.14).

The drag, *D,* and the rolling resistance, *R,* have no *z*- nor *y*-components and oppose the motion of the car.[12] A gravity force component opposes the motion when the car travels up a hill and aids the motion when the car travels down a hill. The lift force has no component along the *x*-axis and so neither opposes nor aids the motion directly. (However, it adds to or subtracts from the net downward force on the car and thus changes the rolling resistance.)

2.20 Example 2.5

Suppose the car in Fig. 2.9 is traveling at a steady 40 kph up the grade. Find the tractive force, wheel torque, and power required to climb the grade.

Solution The tractive force to maintain this speed is the sum of the opposing forces given in Eq. (2.17). The magnitude of the drag, *D,* may be found from the result of Example 2.1 (assuming c_D is constant) by a ratio:

$$D = (57.7\text{N})\left(\frac{40}{96}\right)^2 = 10.0\text{N}.$$

[12] Unless the relative wind blows from behind. This is an unusual situation and will be ignored.

The rolling resistance was found in Example 2.4. So the tractive force is (again neglecting lift):

$$T = 10.0\text{N} + 354.1\text{N} + 13.4\text{N} = 377.5\text{N}.$$

The torque required to climb the grade at 40 kph, assuming the 17.5-in wheel diameter of the Moulton wheels (and ignoring the flattening of the wheel at the contact patch), is:

$$\tau = (377.5\text{N})\left(\frac{17.5\text{in}}{2}\right)\left(0.0254\frac{\text{m}}{\text{in}}\right) = 83.9\text{N}\cdot\text{m}.$$

The total power required at the driven wheel(s) is the tractive force times the speed (m/s), or 4,194.4 W, about 5.6 hp.

2.21 Acceleration

Suppose the vehicle is changing cruising speed. Typical solar car speed changes are gradual; the *y*-axis moment sum and certainly the *z*-axis force sum will remain zero. In this case, the resultant of the *x*-forces equals the *effective mass* (M_e) times the acceleration *(a)*.[13] So the tractive force must now equal

$$T = M_e a + D + R + W_x. \tag{2.18}$$

The tractive work done by the car in traveling a short distance ΔS over which T may be assumed constant is $T(\Delta S)$. Thus, T may be thought of as the tractive work per unit distance.

In order that the reader may begin to develop some intuition about the tractive force, we will study Eq. (2.18). We will assume that the drag coefficient is a constant, which is only approximately true.

Dimension Independence Non-dimensionalizing Eq. (2.18) will make our conclusions independent of, say, the weight of a particular car. We will therefore not calculate *T,* but T/W (T^*). The speed V will be replaced by V/V_D (V^*). The speed scale V_D used to non-dimensionalize the speed will be called the *drag speed*. This is the speed at which the drag force is equal to the weight. (Imagine the car in a stable, nose-first free fall at constant drag coefficient through a uniform atmosphere. The drag speed is the terminal velocity that would be predicted by Eq. (2.17).) It is:

[13] The effective mass is larger than the actual mass and accounts for the need to accelerate masses that translate as part of the body of the car, but also rotate about their own axes, such as the wheels. See Chapter 22.

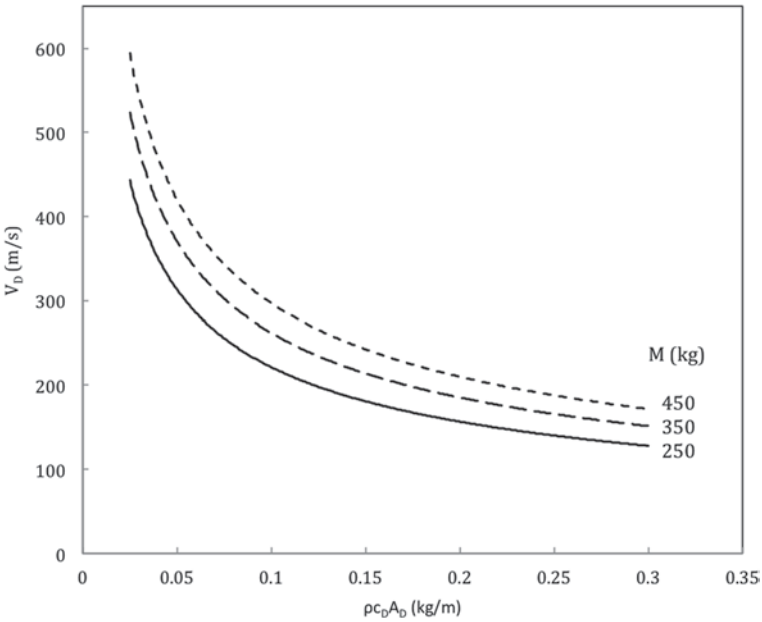

Fig. 2.11 Drag speed

$$V_{\mathrm{D}} = \sqrt{\frac{2W}{c_{\mathrm{D}} A_D \rho}}. \tag{2.19}$$

Using values from Chap. 8 gives $V_{\mathrm{D}} = 237.8$ m/s, or 856 kph (532 mph). Thus, if the car were moving at 88 kph (55 mph), V^* would be 0.103. Figure 2.11 shows how the drag speed is influenced by the vehicle's mass, drag area, and the air density.

The ratio a/g_0 (a^*) will be the nondimensional acceleration. The scale, g_0, is the standard acceleration of gravity (9.807 m/s^2), which we will assume to be uniform over the Earth. Using the models of the forces *R, D,* and W_X previously given and non-dimensionalizing as above, transforms Eq. (2.18) to

$$T^* = \frac{M_{\mathrm{e}}}{M} a^* + D^* + R^* + W_x^*, \tag{2.20}$$

where, if the wind blows from ahead (a numerically negative wind speed),

$$D^* = (V^* - V_W^*)^2, \quad R^* = \mu_1 + \mu_2^* V^*,$$
$$\mu_2^* = \mu_2 V_{\mathrm{D}}, \qquad W_x^* = \sin\alpha.$$

2.22 Steady Motion Studies

No Grade nor Wind The specification in Chap. 8 requires $\mu_1 = 0.004$ and $\mu_2 = 0.0001$ s/m, or $2.78(10^{-5})$ h/km. Using these values, and the other specified parameters given above, let us examine T^*, D^*, and R^* as a function of V^*, with accelaration, no headwind, zero lift, and a horizontal road. Figure 2.12 shows the results of this study. Its quadratic speed dependence causes the drag to be less than the rolling resistance until V^* is approximately 0.075. This corresponds to 64.2 kph (about 40 mph) for the car of Chap. 8. At average speeds characteristic of stop-and-go city traffic, the drag is less than half the rolling resistance. On the other hand, at freeway speeds of 105 kph (65 mph) the drag is more than twice the rolling resistance. The exact crossover speed depends upon the drag speed of an individual car and its rolling resistance coefficients.

Grade Although it has been assumed here for convenience, a horizontal road is rare in reality. Imagine the car is climbing steadily up a 10% grade. The tractive force is increased by 0.099, or the *sin* of the grade angle of 5.71°. This increase in the tractive force is about twice the largest magnitude shown in Fig. 2.12. A 3% grade would increase the tractive force by 0.03. Figure 2.13 shows the tractive force required to climb various grades between 0 and 10% at different speeds.

Also shown in Fig. 2.13 are curves of constant dimensionless power, p^*. This is the power that must be delivered to the driving wheel(s), not the power delivered to

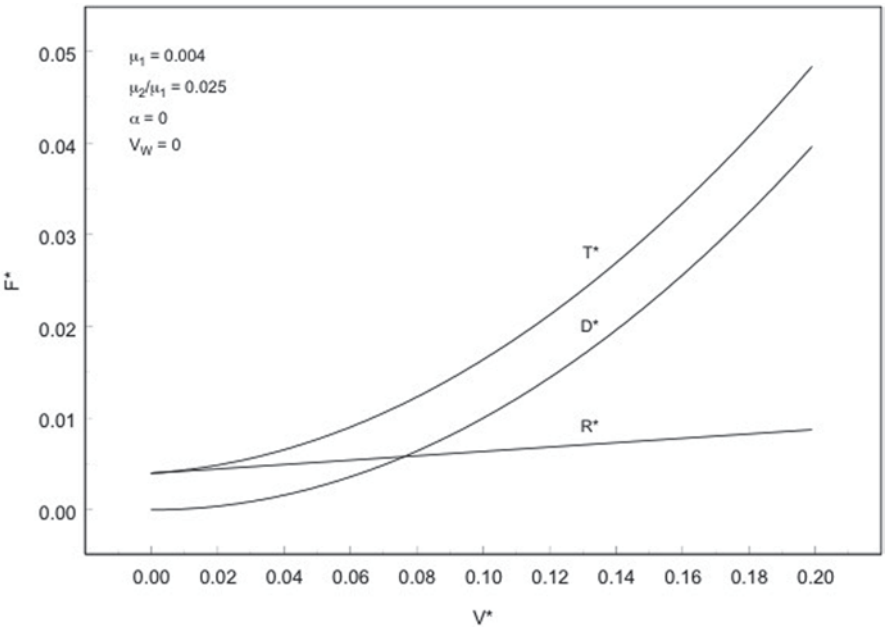

Fig. 2.12 Tractive force components

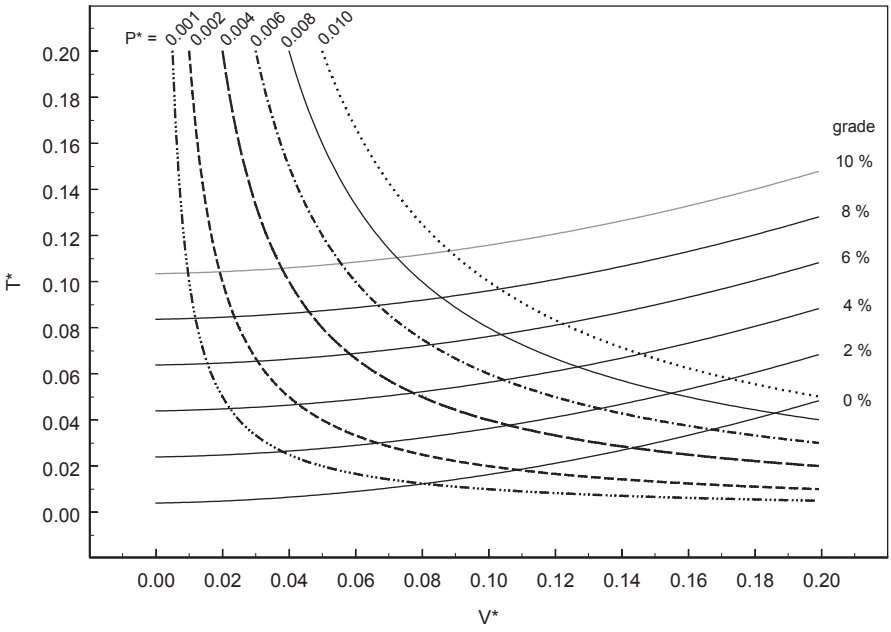

Fig. 2.13 Climbing at steady speed

the motor. The power required to travel at speed V is TV. The dimensionless power is TV/WV_D, symbolized as T^*V^*. The intersection of a power curve with the tractive force curve for a hill gives the climbing speed (found on the abscissa) and the tractive force (found on the ordinate) required to make that speed.

Solar Zone Where do solar racing cars built to Sunrayce specifications fall on the power curves of Fig. 2.13? These cars, because of the solar array and battery limitations imposed by the rules in Chap. 16, can deliver a maximum dimensionless power of roughly 0.006 in full sun (1000 W/m^2)—assuming a drive efficiency of 80%). To do so, they must discharge their batteries at a high rate (say 30 or 40 A). (These rates cannot be sustained for more than a short time without greatly depleting the battery's charge.) If only the solar array is used for power, the cars can deliver roughly 0.001 in full sun. Figure 2.13 shows that the power range 0.001–0.006 means a speed range of about 0.01–0.055 on a 10% grade and 0.08–0.17 on a horizontal road. For the car under study, these dimensionless speeds translate to 9–51 kph (about 6–32 mph) and 60–146 kph (about 37–91 mph), respectively.

Strategic Decision What goes up must come down, at least eventually. So it is possible to recover some of the energy expended to overcome gravity when climbing a hill, as gravity helps to accelerate the car on the following downhill grade.[14] The

[14] Only some of the energy expended is recoverable because of the losses in the battery and the drive. This will be discussed in more detail in Chap. 4, *Storing Energy,* and Chap. 5, *Electric Motor Drives*.

racing team must decide whether to return a portion of the energy to the battery through regeneration (running the motor as a generator) or to use it all to gain speed.

2.23 Wind and Drag

Headwind Suppose that the headwind of 8 kph specified in Chap. 8 is blowing. Because of the high drag speed of the car under study, the dimensionless relative wind speed is increased by only 0.0093. Nevertheless, for a horizontal road, Fig. 2.13 shows that at 88 kph (55 mph), the drag, and therefore the tractive force, is increased by about 19%.

Wind Averaging As Kurtz (1980) pointed out, real vehicles seldom operate exclusively at zero yaw; there is usually a crosswind. Hence, if a single drag coefficient is to be used in design, it must be the wind-averaged value. But to calculate this value, the relative wind speed and direction and the car's speed and course must be known at any moment, and the drag coefficient must be known as a function of the yaw angle. The design weather and route supply the former, but wind tunnel tests on models, at least, or coast-down tests with the full-scale car provide the best measurement of the latter.

Drag and Yaw Figure 2.14[15] shows the drag coefficient as a function of the yaw angle for a passenger car typical of those tested by Kurtz (1980) and a properly designed solar racer similar to the *Spirit of Biel* reported by Storey et al. (1994). The drag of the passenger car increases with yaw, whereas the drag of the solar racer has the opposite tendency. Therefore, the wind-averaged drag of the solar racer will be less, and the wind-averaged drag of the passenger car will be greater than its drag coefficient at zero yaw.

The yaw angle and speed of the relative wind over the solar racer at any moment depend on the racer's course and speed and the wind's speed and direction. Kurtz (1980) reported wind-weighting factors for estimating the effective drag coefficient of passenger cars from their drag coefficients at zero yaw angle for several standard driving cycles.[16] Kurtz's factors will not apply to streamlined solar cars with falling drag coefficients.

Illustration Figure 2.15 was prepared to illustrate the error in using the zero-yaw drag coefficient for a solar car assumed to have a falling drag-yaw characteristic similar that illustrated in Fig. 2.14.[17] The car was assumed to be driving due west at

[15] The curves were normalized to their respective drag coefficients at zero yaw because the drag coefficient of the typical passenger car over the yaw angle range displayed was three to five times that of the solar racer.

[16] The results showed that the weighting factor could vary from about 1.04 (a 4% correction) to more than 1.4 (a 40% correction), depending upon the driving cycle and the vehicle's drag characteristics.

[17] Other parameters: M_e, 338 kg; μ_1, 0.004; μ_2, 0.0001 s/m, A_D, 1.45 m^2.

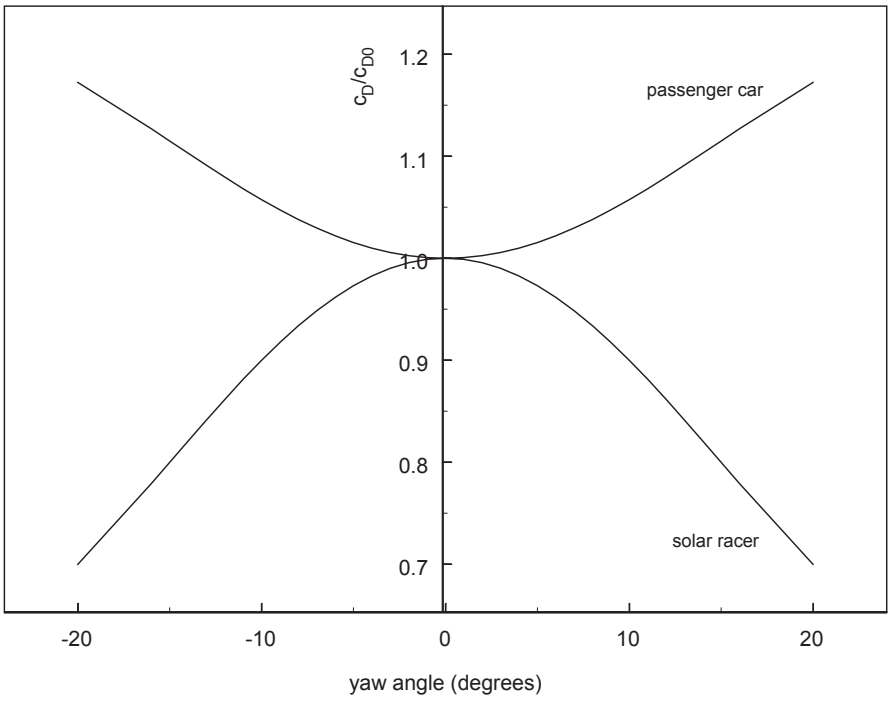

Fig. 2.14 c_D/c_{D0} as a function of yaw

various constant speeds on a level road under standard conditions. The wind speed and direction were taken as 8 kph and 225°, respectively. The Reynolds number dependency of the drag coefficient of the smooth, streamlined solar car was taken to be similar in shape to that of the 2:1 ellipsoid of Fig. 2.6.

Operating Zone The speed in the study ranged from 1.0 to 88 kph. Observe that even at low speeds the resulting Reynolds number placed the car after the laminar–turbulent transition. And if there had been no wind, the Reynolds number at low speeds would have been about 10^5, just before the transition to turbulence. During periods of acceleration from rest, the car would traverse the drag coefficient curve to the turbulent region in seconds. This transition shifts to somewhat lower Reynolds numbers as the vehicle's basic shape becomes more streamlined, as Fig. 2.6 implies.

The foregoing discussion supports this design thumb rule: A solar car may be assumed always to operate in the turbulent, separated-flow region. Notice that the zero-yaw drag coefficient in this region increases relatively slowly with the Reynolds number because of increasing skin friction drag. Remember, however, that the thumb rule applies to the car as a whole. The local flow over upstream areas of the car, such as a canopy, may still be laminar separated, or, near the nose, just laminar.

Force Error Figure 2.15 shows the percent relative error in the calculated tractive force compared to the yawed case as a function of the Reynolds number. A maximum error of about 3 % appears near the point at which the speed and yaw angle curves

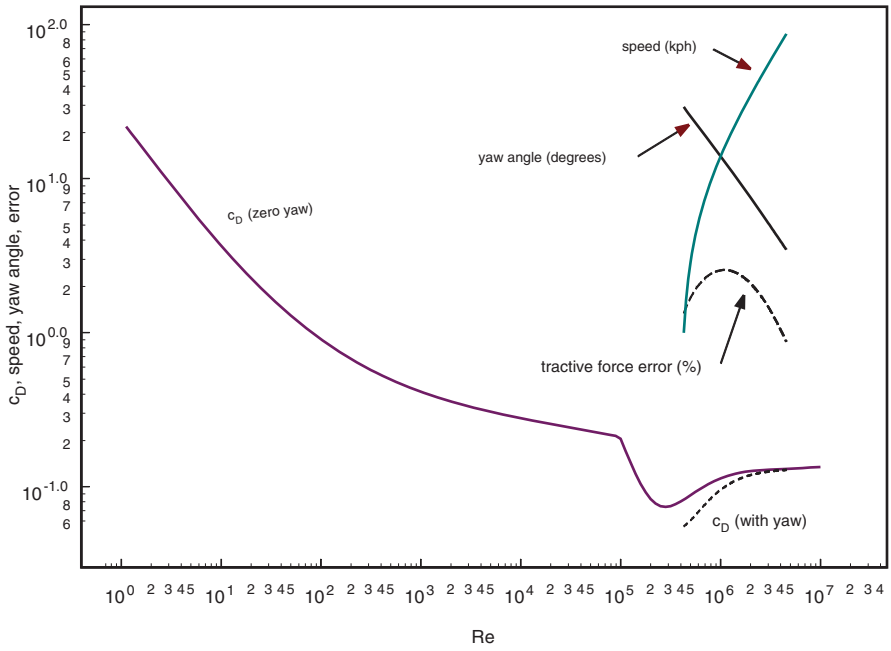

Fig. 2.15 Error from neglect of yaw

cross. At low speeds, the yaw angle is at its largest, but the quadratic dependence of the drag on the relative wind speed forces the drag to be small compared to the rolling resistance. Hence, the error is small. But as the speed increases, the importance of the drag exceeds that of the rolling resistance, as Fig. 2.12 shows. But the yaw angle is decreasing. These competing influences cause the error to pass through a maximum and decrease until it is again about 1 % at 88 kph vehicle speed. Higher wind speeds, or wind directions further south, increase the error. For example, doubling of the error is possible at wind speeds of 16 kph (10 mph).

2.24 Unsteady Motion Study

Steady conditions are uncommon (though simpler to analyze). The car is usually driving into an upgrade or a downgrade or into some other condition affecting its motion. Thus, the speed and torque are usually changing as functions of time. Equation (2.20) can be used to find the speed as a function of time. The time dependence of the torque (tractive force) must be known, however.

Little Taps If the acceleration were constant, the speed at the end of a time interval would be:

$$V_2 = V_1 + a_1(t_1 - t_2). \tag{2.21}$$

We stipulate that the time interval be small enough so that the acceleration is approximately constant over the interval: The car moves in little steps, as if tapped by a hammer. Then we can compute the speed at the end of each time interval from the speed at the end of the previous time interval using Eq. (2.20). In this way, we march forward in time.

2.25 Example 2.6

Calculate the velocity as a function of time for a car accelerating from 40 to 88.5 kph with the tractive force set equal to that required to sustain 88.5 kph and also four times that value. The road is horizontal.

Solution The tractive force corresponding to 88.5 kph is:

$$T = \frac{1}{2} c_{\mathrm{D}} A_D \rho V_2^2 + (\mu_1 + \mu_2 V_2) W = (0.5)(0.11\mathrm{m}^2)\left(1.18\frac{\mathrm{kg}}{\mathrm{m}^3}\right)\left(24.58\frac{\mathrm{m}}{\mathrm{s}}\right)^2 + \left(0.004 + 0.0001\frac{s}{\mathrm{m}} \times 24.58\frac{\mathrm{m}}{\mathrm{s}}\right)(3315\mathrm{N}) = 58.57\mathrm{N}.$$

At the instant before the car begins to accelerate,

$$D_0 = (0.5)\left(0.11 m^2\right)\left(1.18\frac{kg}{m}\right)\left(11.11\frac{m}{\mathrm{sec}}\right)^2 = 8.012N,$$

$$R_0 = \left(0.004 + 0.0001\frac{\mathrm{sec}}{m} \times 11.11\frac{m}{\mathrm{sec}}\right)(3315\,N) = 16.943N.$$

Therefore, taking $M_e/M = 1.05$, the acceleration is:

$$a_0 = \frac{T - D_0 - R_0}{M_{\mathrm{e}}} = \frac{58.57\mathrm{N} - 8.012\mathrm{N} - 16.943\mathrm{N}}{354.9\mathrm{kg}} = 0.0947\frac{\mathrm{m}}{\mathrm{s}^2},$$

and the speed after a time step of 1.0 s is:

$$V_1 = V_0 + a_0 \Delta t = 11.11\frac{\mathrm{m}}{\mathrm{s}} + \left(0.0947\frac{\mathrm{m}}{\mathrm{s}^2}\right)(1.0s) = 11.205\frac{\mathrm{m}}{\mathrm{s}}.$$

Table 2.2 gives the results for the first 3 s. As illustrated above, the acceleration used to predict the next speed is found from the previous speed. The power delivered to the wheel, the product of the tractive force and the speed, is shown in the last column.

Figure 2.16 shows curves of velocity as a function of time for the required speed increase on a horizontal road with no headwind. The curve resulting from applying four times the first tractive force is also shown for comparison.

Table 2.2 Acceleration under constant tractive force

t(s)	V (m/s)	D (N)	R (N)	a (m/s^2)	P (W)
0	11.11	8.012	16.943	0.0947	277.3
1	11.205	8.160	16.974	0.0942	656.3
2	11.299	8.299	17.006	0.0937	661.8
3	11.393	8.437	17.037	0.0933	667.3

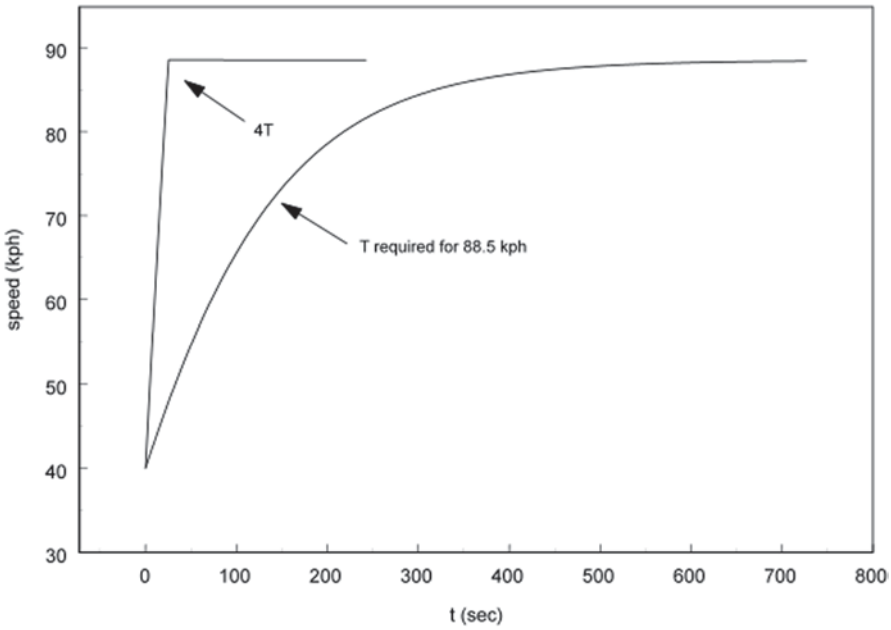

Fig. 2.16 Accelerated motion

References

Gillespie, T. D. (1992). *Fundamentals of vehicle dynamics*. Pennsylvania: Society of Automotive Engineers.

Hucho, W.-H. (1978). The aerodynamic drag of cars, current understanding, unresolved problems, and future prospects. In G. Sovran, T. Morel, & W. T. Mason (Eds.), *Aerodynamic drag mechanisms of bluff bodies and road vehicles* (p. 1). New York: Plenum Press.

Hucho, W.-H. (1987a). Aerodynamics of passenger cars. In W.-H. Hucho (Ed.), *Aerodynamics of road vehicles* (p. 106). London: Butterworth and Co. Ltd.

Kurtz, D. W. (1980). *Aerodynamic design of electric and hybrid vehicles, a guidebook*, N81–12943 (NASA-CR-163744 Jet Propulsion Lab) NTIS 1980.

Kyle, C. R. (1990). The sunraycer: Wheels, tires, and brakes. In P. MacCready et al. (Eds.), *Sunraycer case history*. Society of Automotive Engineers, lecture 3–3.

Morelli, A. (1983). Aerodynamic basic bodies suitable for automobile applications. *Int. J. of Vehicle Design*, Technological Advances in Vehicle Design Series, SP3. In M. A. Dorgham (Ed.), *Impact of aerodynamics on vehicle design* (p. 70). United Kingdom: Interscience Enterprises Ltd., La Motte Chambers.

SAE. (1997) Road load measurement and dynamometer simulation using coastdown techniques. SAE J1263 Feb. 96, *1997 Society of Automotive Engineers Handbook* (Vol. 2, p. 26.531).
Sherman, F. S. (1990). *Viscous flow*. New York: McGraw-Hill.
Steeds, W. (1960). *Mechanics of road vehicles*. London: Iliffe and Sons, Ltd.
Storey, J. W. V., Schinckel, A. E. T., & Kyle, C. R. (1993). *Solar racing cars*. Canberra: Australian Government Publishing Service.
White, F. M. (1986). *Fluid mechanics*. New York: McGraw-Hill Book Company.